

Experimental and numerical modelling of a oscillatory jet thrust vectoring system

by

M.P. Arruda⁽¹⁾, N.J.Lawson⁽²⁾ and M.R. Davidson⁽³⁾

Department of Aerospace, Power & Sensors, Cranfield University, Shrivenham SN6 8LA, U.K.

⁽¹⁾E-Mail: mauro_arruda@hotmail.com

Cranfield University, College of Aeronautics, Cranfield MK43 0AL, U.K.

⁽²⁾E-Mail: n.lawson@cranfield.ac.uk

Dept. of Chem. and Biomol. Eng., The University of Melbourne, Victoria 3010, Australia

⁽³⁾E-Mail: m.davidson@unimelb.edu.au

ABSTRACT

In the following, an innovative method is presented for control of an oscillatory turbulent jet in a thin rectangular cavity with a depth to width ratio of 0.16. In this case jet thrust vectoring is achieved by mass injection of a secondary jet into the region above the primary jet nozzle exit and perpendicular to the primary nozzle axis. Without injection the primary jet in the cavity attains a natural period of oscillation in the transverse cavity plane driven by the recirculation zones bounding the jet and a feedback loop between the two zones. Secondary injection, however, stabilises the jet position in the cavity thus allowing primary jet thrust vectoring. An experimental model, a 2D and a 3D Fluent computational fluid dynamics (CFD) model are used to investigate the flow characteristics under various secondary injection mass flow rates and injection positions. Two-dimensional laser Doppler anemometry (LDA) measurements are compared to Fluent 2D and 3D CFD models with a standard $k-\epsilon$ turbulence model and a realizable $k-\epsilon$ model. Experimental results show that deflection angles (δ) of up to 17° for 25% relative secondary momentum (β) are possible (Figure 1). The key to high jet control sensitivity is found to be lateral jet momentum with the optimum injection position at 12% of the cavity length from the top of the cavity. Results from the CFD model also show a standard $k-\epsilon$ turbulence closure with non-equilibrium wall functions provides the best predictions of the flow.

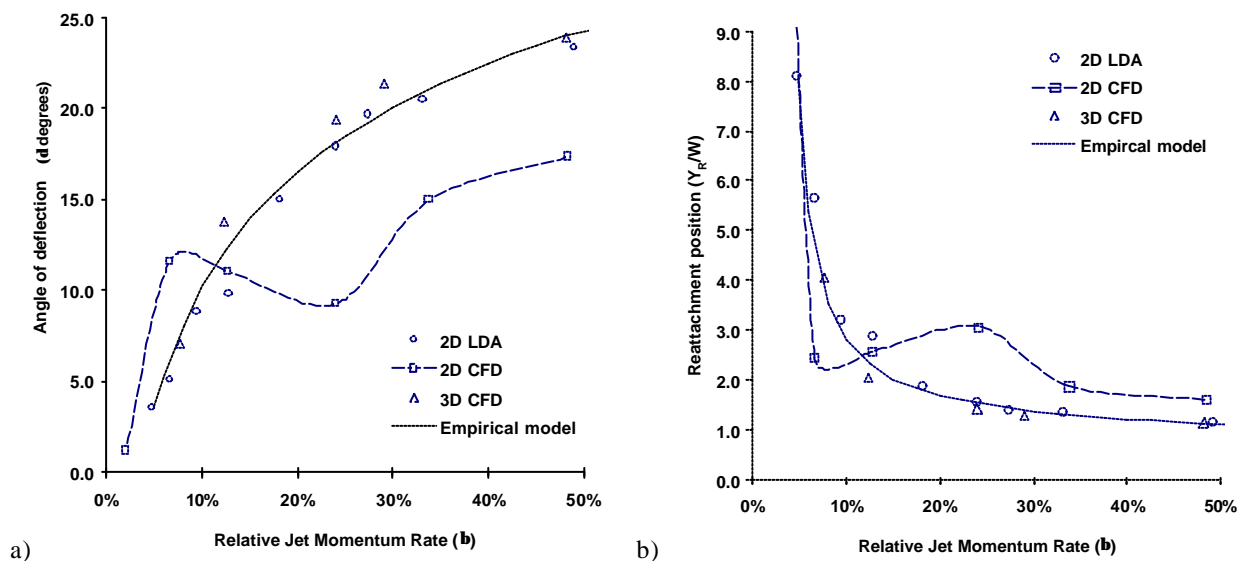


Fig. 1. thrust vectoring characteristics for injection relative momentum \mathbf{b} vs a) primary jet deflection angle \mathbf{d} b)
primary jet attachment point Y_R/W

1. INTRODUCTION

Numerous studies on fluidic flow control and more specifically on thrust vectoring have been published for high Reynolds number flows (see Schmid et al 2000; Alvi et al 2000). These turbulent flows have shown to be highly sensitive to shear and boundary layer disturbances that are amplified and convected downstream and their control has been explored with new systems based on mixing layer excitation for thrust vectoring, jet mixing and spreading enhancement (e.g., Smith and Glezer 1997, Raman et al 1994, 1997; Pack and Seifert 2001, Miller et al. 1999). However, flow vectoring systems by secondary injection for low Reynolds number flows (laminar and turbulent) have received limited attention. The current investigation is concerned with the study of a jet flow vectoring control system with potential application to both laminar and turbulent flows. This control method would be applicable to applications such as MAV's (Micro-Air-Vehicles) and UAV's (Unmanned-Air-Vehicles). The system uses a simple oscillatory confined jet flow generated from a submerged entry nozzle (SEN) placed in a thin rectangular cavity with vectoring control by lateral secondary injection.

Confined turbulent jets often exhibit oscillations which are amplified and self-sustained for certain flow conditions and cavity geometries as reported by Rockwell (1983), Rockwell and Naudascher (1978, 1979). Self-sustained cavity jet oscillations are strongly influenced by shear-layer instabilities or other lower frequency mechanisms which have a disturbance feedback. These flow oscillations can be categorized into three different groups: fluid dynamic, fluid resonant and fluid elastic.

The current study is concerned with the natural fluid dynamic oscillation phenomenon inside a thin rectangular cavity, whereby a submerged jet exhibits an oscillatory motion across the broad face of the cavity. Here the frequency of oscillation is around two orders of magnitude less than that of the shear-layer instability and the mechanism of oscillation is known to rely on the interaction between the two major recirculation zones formed between the main jet and the cavity sidewalls. Lawson and Davidson (2000, 2001) and Shakouchi et al. (1982, 1986) have considered the mechanism for this type of oscillatory flow and have highlighted the importance of a feedback loop which provides mass exchange from one side of the cavity to the other and which connects the two major recirculation regions. They have also shown that stable oscillations will only occur for particular cavity dimensions and that the frequency of oscillation is proportional to the inlet jet velocity and inversely proportional to cavity width. Thus the jet oscillation frequency f can be simply characterised by a Strouhal number S_{t,l^*} based on a cavity length scale (l^*), usually the cavity width (W) or the inlet nozzle diameter (d_i) and the mean jet velocity V such that:

$$S_{t,l^*} = \frac{f l^*}{V} \quad (1)$$

Given that jet deflection angle will depend on the position of the main pair of eddy structures confining the jet, control of these structures offers a method by which the jet can be vectored. This approach is the basis of the flow control method demonstrated in the present paper. In such a flow control system one must obtain the maximum jet deflection possible for the minimum secondary mass flow injection. This requirement is investigated by using a combined approach of computational fluid dynamics (CFD), both 2D and 3D, and experimental modelling. The experimental approach is based on a physical model and laser Doppler anemometry (LDA) (see Durst et al 1981) measurements. Initial results have isolated the most important control variables and have allowed recommendations to be made for an optimum configuration including secondary jet injection position and required jet characteristics.

2. NUMERICAL MODELLING

2.1 Model Formulation

Two-dimensional and three-dimensional CFD models of the cavity flow with lateral injection are described and the flow predictions compared with 2D LDA measurements of the flow. The commercial CFD solver ©FLUENT and mesh builder

©GAMBIT were used to develop the transient models of the cavity jet flow. Both 2D and 3D transient models were tested with two different $k-\epsilon$ turbulence models (the standard $k-\epsilon$ model as proposed by Launder and Spalding (1972) and the realizable $k-\epsilon$ model as proposed by Shih et al. (1995)), using either standard (Launder and Spalding, 1974) or non-equilibrium (Kim and Choudhury, 1995) wall functions (newf). Model solutions were validated against 2D LDA flow measurements by consideration of the dominant period of oscillation, the mean velocity decay along the centreline of the primary jet and mean velocity transverse profiles downstream of the nozzle.

2.2 Model Layout

The 2D model was developed using a $250\text{mm} \times 585\text{mm}$ rectangular domain as shown in Figure 2. No-slip conditions were specified at top and side boundaries. The inlet flow was modelled by an internal mass source (see Figure 2) after Gerbert *et al.* (1998) and resistance to cross-flow resulting from the obstruction caused by the nozzle was introduced in the 2D model by adding a resistive force (R) in the cross flow region above the nozzle in the form $R=K|V|V$, where the resistive coefficient (K) is defined by $K = 0.594r/d_i$ (Lawson and Davidson 2001). An internal wall with slip conditions was defined on the upper face of the primary source region to ensure that the flow in this region is always directed outwards into the cavity in a manner consistent with an actual nozzle exit (see Figure 2). At the bottom boundary a constant pressure distribution of $P_{\text{outlet}}=0$ was defined.

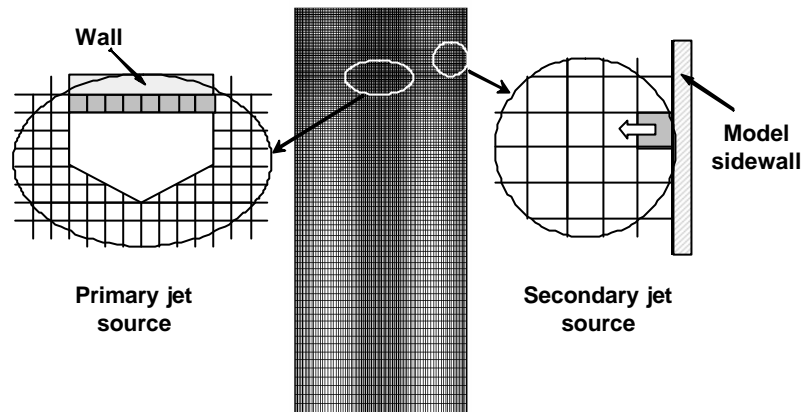


Fig. 2. 2D (182 \times 232) and 3D CFD (102 \times 130) model front view of mesh configuration and source region

The 3D model consisted of a $250\text{mm} \times 585\text{mm} \times 40\text{mm}$ rectangular domain with no-slip conditions at all solid walls including those of the SEN which is now explicitly represented. The SEN was modelled as a cylindrical volume with a $1/7^{\text{th}}$ power law velocity profile and a turbulence intensity I of $I=6.0\%$ at the nozzle exit. At the bottom boundary a constant pressure distribution of $P_{\text{outlet}}=0$ was defined. The computational mesh in a horizontal plane through the 3D domain is shown in Figure 3.

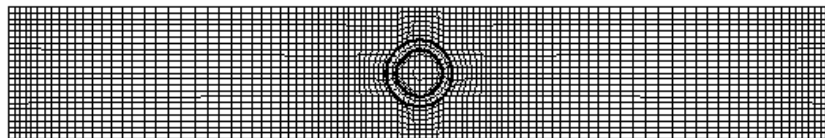


Fig. 3. 3D CFD model top view of mesh (102 \times 22)

The lateral control jets were modelled by defining mass and momentum sources in cells within the lateral injection as shown in Figure 2. The desired mass flow was added in the assigned source cells and then accelerated up to the average velocity of the actual control jet with no additional turbulence kinetic energy or dissipation rate.

The 2D and 3D front-view meshes in the jet region were refined using a geometric progression distribution. In the 3D model a uniform structured mesh was applied at the top and bottom sections. Both models used QUICK differencing and SIMPLEC pressure-velocity coupling. Grid independence was achieved by running the model with 44% more $x-y$ cells which resulted in approximately 4% increase in the period of oscillation. Near-wall cell dimensions are such that

computed y^+ is always less than 140, which is within the maximum recommended value of 200 for the use of wall functions in turbulent flow calculations (see Fletcher 2001).

A transient solver with a first order implicit time stepping was used to predict the flow field inside the cavity. The time step was set to $\Delta t=0.01s$. Reducing the time step to 0.005s resulted in less than 2% difference in the period of oscillation. Typically 10-20 iterations led to a convergent solution at each time step with normalised residuals of less than 0.1%. The realizable k- ϵ based models also resulted in a typical increase in computing time of 27% when compared to the standard k- ϵ models.

3. PHYSICAL MODELLING

3.1 Experimental rig

A 5mm thick glass-walled rectangular cavity with dimensions of 250mm \times 585mm \times 40mm was constructed for maximum optical access. The main jet was generated by a submerged, glass-walled, cylindrical SEN tube driven by a closed water circuit and a 0.160m³ water tank mounted 1.5m above the cavity (Figure 4). The SEN, with diameters of $d_{i,1}=14mm$ and $d_{o,1}=20mm$ was mounted through the top of the cavity and had an effective submergence of $S=95mm$. The SEN length of $L=100mm$, corresponding to $L/d_i=84$, ensured fully turbulent flow. Use of a header tank isolated any pump fluctuations from the main jet and a gate valve positioned immediately after the tank outlet was used to control the SEN flow rate. The header tank was supplied from a reservoir and two centrifugal water pumps with powers of 45W and 250W with its level been maintained using an overflow drainpipe back to the reservoir. A second 250W centrifugal water pump in the reservoir was used to supply the lateral injection jet through a perspex sidewall. Adjustment of this jet flow rate was achieved using a gate valve installed on the pump outlet and three lateral nozzles with different inner diameters ($d_{i,2}=5mm$, $d_{i,2}=6mm$, $d_{i,2}=7mm$) were used to test a range of injection mass flow rates and momentum fluxes.

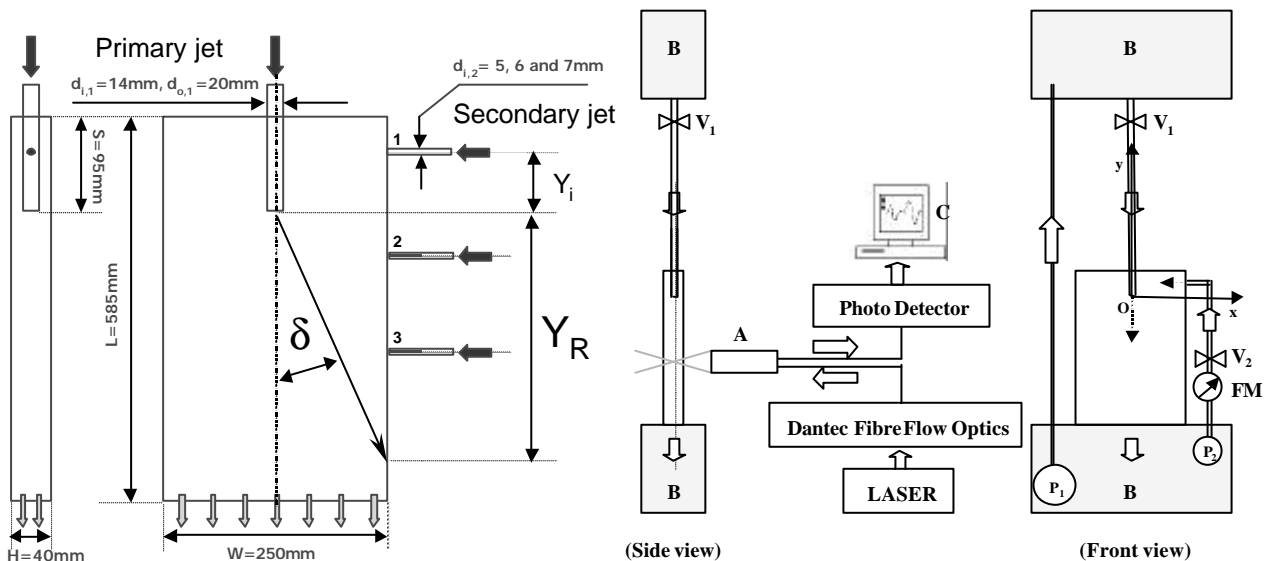


Fig. 4. Experimental set-up for thrust vector modelling

The flow rate through the cavity was controlled by adjusting an outflow slot valve as outlined by Lawson and Davidson (2001). Any mismatch in flow rates between the SEN and cavity outlet was detected using an additional 2mm diameter overflow tapping at the top of the cavity which would indicate a raise or fall in static pressure inside the cavity.

The rig instrumentation was a static pressure tap system on the SEN supply line to monitor flow rate and a volumetric flow meter installed upstream of the lateral jet injection point. Calibration curves for both flow monitors were generated from data collected by measuring the time taken to collect a known volume of water in a secondary container.

3.2 Flow measurement system

A 2D Dantec Fibreflow backscatter LDA system with two BSA Enhanced processors was used for the flow velocity and turbulence measurements inside the cavity. The green (514.5nm) and blue (488nm) beams were used for the two measurement components with a 310mm lens corresponding to a measurement volume of $0.047\text{mm} \times 0.047\text{mm} \times 0.381\text{mm}$. Flow seeding was with glass micro-spheres of diameter 30-50 μm . An in-house $1.25\text{m} \times 0.7\text{m} \times 0.5\text{m}$ x-y-z traverse was used to move the probe around a pre-programmed grid. Typical velocity sample sizes were set to 32 with a maximum acquisition period of 30s giving an average data rate of 1000Hz. These settings ensured adequate temporal resolution for the oscillatory frequencies analysed. The u and v velocity data were subsequently processed into mean and rms values with errors of between 4.2% - 9.6% using methods outlined by Lawson & Davidson (1999).

3.3 Flow measurements

Figure 5 shows the major variables of interest for the flow control study. Given primary and secondary nozzle average exit velocities and mass flows of V_1, \dot{m}_1 and V_2, \dot{m}_2 respectively, the ratio β of secondary jet momentum $\dot{m}_2 V_2$ rate to primary jet momentum $\dot{m}_1 V_1$ will be used throughout the subsequent discussion as follows:

$$b = a \frac{V_2}{V_1} \quad (2)$$

where α is the mass flow ratio $a = \dot{m}_2 / \dot{m}_1$. As the primary jet is curved due to its interaction with the pair of recirculation zones, three angles, d_1, d_2 and d , are used to define the vectoring characteristics of the jet. Thus the first angle d_1 is defined about the primary jet exit centreline and an intermediate point determined from the jet velocity profile at $y/W = -0.6$ and the second angle d_2 is defined about the d_1 endpoint and the sidewall attachment point Y_R . The third angle d is defined about the primary jet exit centreline and the sidewall attachment point Y_R . This point is analogous to an average angle of d_1 and d_2 and will correspond to zero when the attachment point Y_R is infinity. To precisely locate the d_1 and d_2 angles, the centroid of the primary jet profile is taken such that:

$$d_1 = \arctan \left[\frac{1}{2 \cdot Y_p} \cdot \frac{\sum_{i=2}^N [(X_i^2 - X_{i-1}^2)(v_i + v_{i-1})]}{\sum_{i=2}^N [(X_i - X_{i-1})(v_i + v_{i-1})]} \right] \quad (3)$$

$$d_2 = \frac{1}{N} \sum_{i=1}^N \arctan \left(\frac{u_i}{v_i} \right) \quad (4)$$

where Y_p is the downstream position of the horizontal line of measured points ($Y_p = 0.6W$), X_i the horizontal position of the measured point ($X_i \in [-0.45W; 0.45W]$) and u and v are the velocity components in the cross-stream and downstream directions, respectively. N is the number of measured points ($N=19$) such that:

$$Y_R = \frac{0.5W - 0.6W \cdot \tan(d_1)}{\arctan(d_2)} + 0.6W \quad (5)$$

$$d = \arctan \left(\frac{0.5W}{Y_R} \right) \quad (6)$$

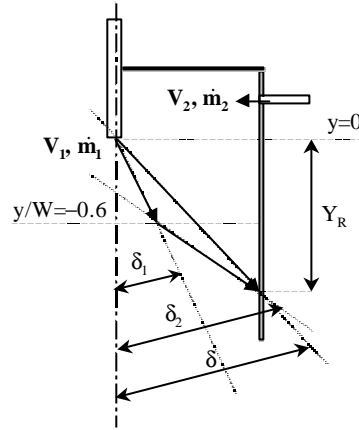


Fig. 5. Schematic of flow control variables

Full field measurements were made at the central plane across the cavity with $0.05W \times 0.05W$ ($W = 250\text{mm}$) of grid spacing and on a transverse line of 19 points at $y/W = -0.6W$ below the nozzle exit with $0.05W$ of grid spacing. In addition, primary and secondary jet velocity and turbulence components were measured at the centre of primary and secondary nozzle exits.

4. RESULTS AND DISCUSSION

4.1 Primary jet characteristics without injection ($b = 0$)

A monitoring point positioned at $y/W = 0.18$, $z/W = -0.05$ was used to check the baseline oscillatory characteristics, i.e. with no secondary injection ($\beta = 0$), for all the turbulence models tested for the 2D and 3D CFD models. The same monitoring point was also used to record the LDA data from the physical model (here the z coordinate is measured from the central x - y plane and is perpendicular to it). Although the flow was observed to be highly transient, with reference to Figure 6, all the tested CFD solutions resulted in a stable oscillation of the primary jet flow. Of the 2D and 3D newf solutions, the 3D solution appears to more accurately capture some of the shorter timescale characteristics of the oscillation as well as the primary jet oscillation period. The oscillatory behaviour is dominated by flow exchanges in the x -direction and as described by Shakouchi *et al.* (1986) and more recently by Lawson and Davidson (2001). The period of oscillation was found to be approximately of $T = 5.0\text{s}$ ($S_{t,w} = 0.013$).

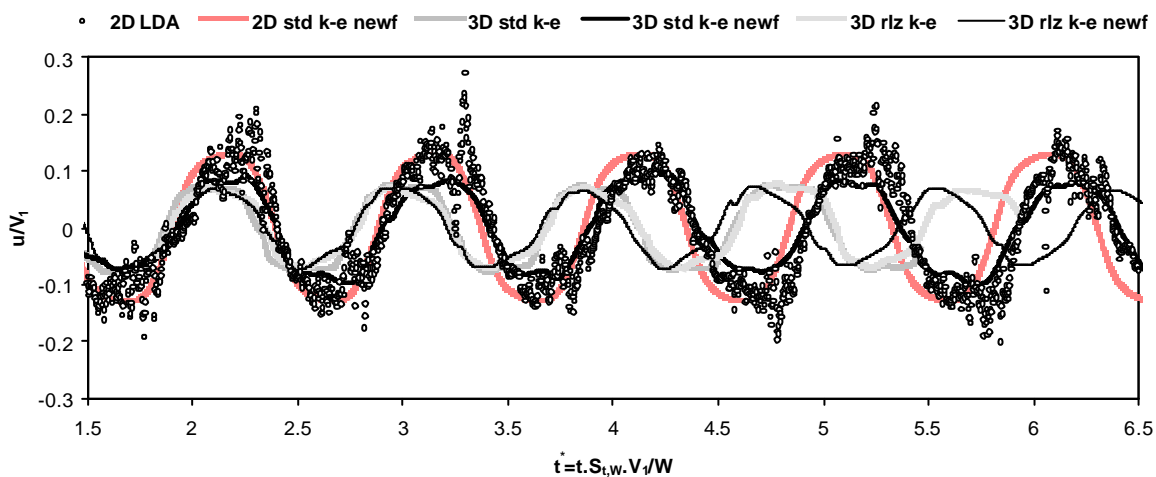


Fig. 6. Primary jet cross flow characteristics ($b = 0$, $V_1 = 3.75\text{m/s}$)

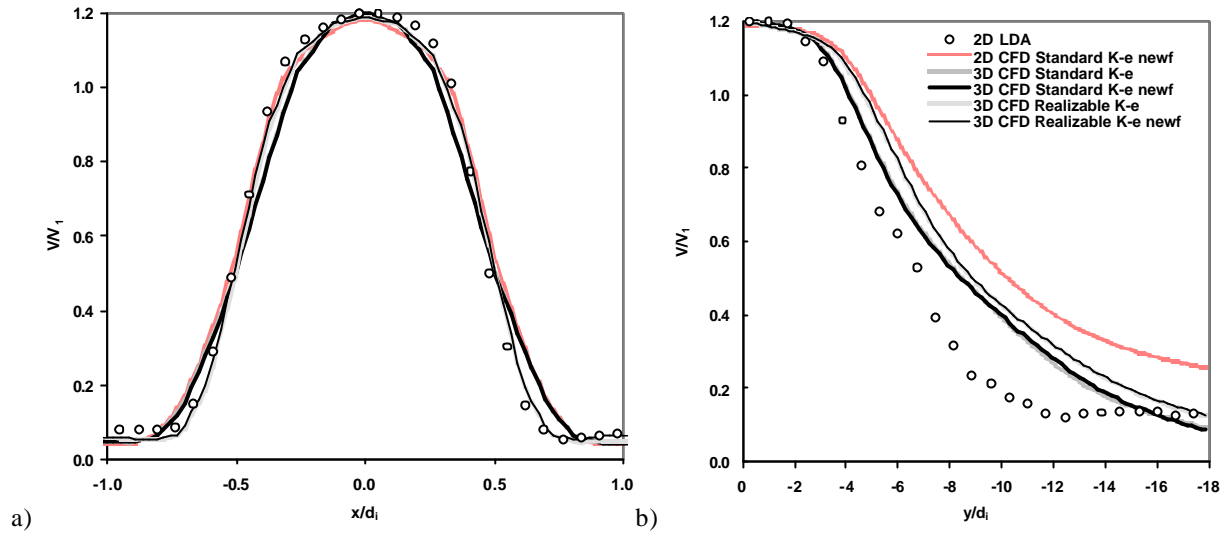


Fig. 7. Primary jet cross flow characteristics b) transverse jet profile ($y/d_1 = -1.35$) c) Centreline jet profile ($b = 0$, $V_1 = 3.75\text{m/s}$)

The LDA centreline turbulence intensity at the nozzle exit was found to be $I_1=6.0\%$, i.e. greater than that for a fully developed pipe flow (3.7%). This discrepancy, however, is attributed to the jet primary oscillation close to the nozzle exit which the theoretical value will not account for. Comparisons in Figure 6 suggested that the best 2D and 3D CFD results were obtained using the std k- ϵ newf model. However, further consideration of both the oscillation period and the jet profiles shown in Figure 7 found the best overall results to be obtained by using the std k- ϵ model. In this case the CFD results matched the LDA results to within 5% of V_1 .

4.2 Primary jet flow time-averaged characteristics with injection ($b>0$)

In order to investigate the primary jet dependence on secondary jet injection position, time-averaged LDA data was recorded from the centreline plane for three secondary injection positions, $Y_1/W = 0.12$, $Y_2/W = -0.28$ and $Y_3/W = -0.68$. These positions corresponded to injection points above the jet into the cross flow region and below the jet at the middle and bottom areas of the cavity. Figure 8 shows the LDA vector plots for all three cases where it can be seen that primary jet deflection has been achieved for every injection position.

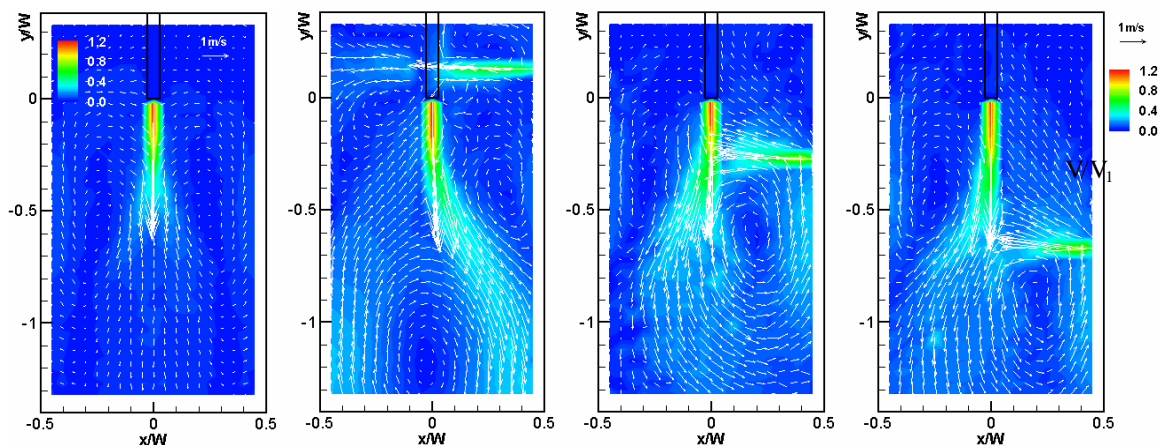


Fig. 8. 2D LDA mean flow velocity vectors with secondary injection at three different positions along the cavity sidewall a) $b = 0$ b) $b = 49\%$, $Y_1/W = 0.12$ c) $b = 38.1\%$, $Y_2/W = -0.28$ d) $b = 40.7\%$, $Y_3/W = -0.68$

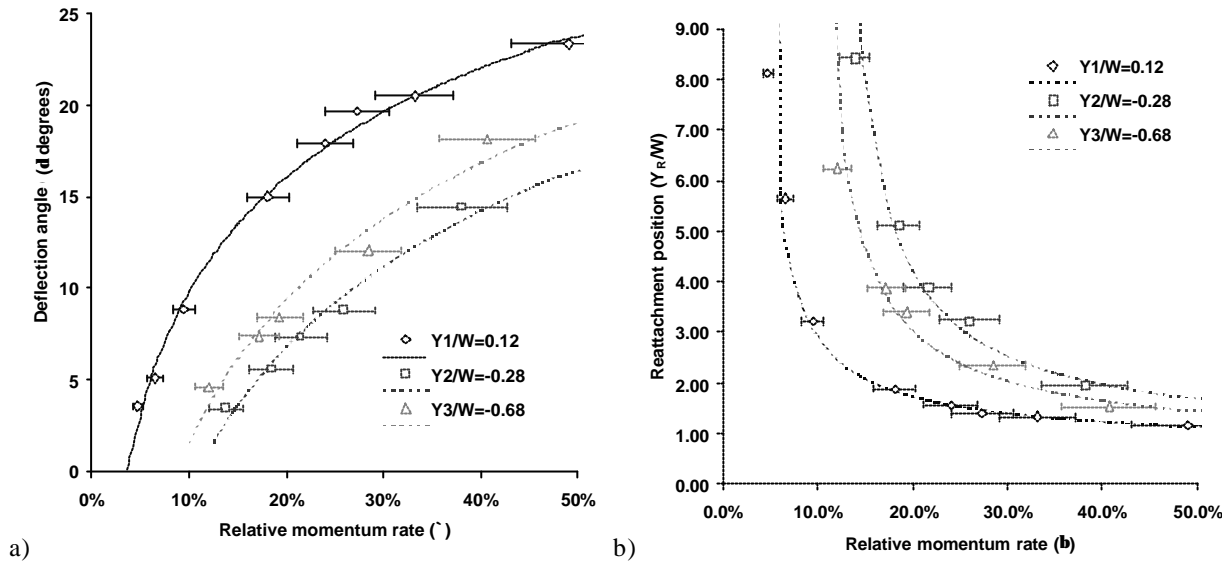


Fig. 9. 2D LDA data showing a) deflection angle b) attachment point characteristics with varying Y_1/W

The primary jet deflection angles δ however, are proportionately less with respect to β for the injection cases below the nozzle than for the injection above the nozzle. For example, $Y_2/W = -0.28$ yields predicted values $\beta = 38.1\%$, $\delta = 14.4^\circ$ whereas when $Y_1/W = 0.12$, the model predicts $\beta = 49\%$, $\delta = 23.3^\circ$. Thus it appears the injection position above the nozzle is offering greater control sensitivity. This finding is further reinforced in Figure 9 which shows overall plots from LDA data of deflection angle δ versus relative injection momentum β . Here it can be seen that at an equivalent value of β , deflection angles δ can be as much as 500% higher at $Y_1/W = 0.12$ than at $Y_2/W = -0.28$. At higher values of β the difference becomes less, for example δ is 65% higher at $\beta = 40\%$ compared to 500% higher at $\beta = 15\%$. Therefore in every case greater performance is being achieved by injection above the nozzle. It must also be noted that the jet direction changes with injection position. Thus primary jet deflection occurs towards the side of injection when injecting above the nozzle and to the opposite side of injection when injecting below the nozzle. This characteristic reflects the different thrust vectoring mechanisms where injecting above the nozzle is through feedback control and below the nozzle is by forced deflection of the jet through momentum addition.

Given the greater thrust vectoring performance with secondary injection above the nozzle, CFD results are now presented in Figure 10 for $Y_2/W = 0.12$ for the 2D and 3D models. Initial comparisons with the LDA data in Figure 8 appear to show both the 2D and 3D models to closely match the experimental results in terms of primary jet position. However, if the 2D and 3D model characteristics are now considered in more detail, across a large range of secondary injection β , the 2D prediction gives unacceptable results. This is illustrated by examining the characteristics of δ and Y_r/W vs β in Figure 1a and 1b. In this case the magnitude of deflection of the 2D model is not comparable to the LDA results. There is a noticeable divergence in the trend for the 2D CFD between $\beta = 5\% - 35\%$ where the deflection angle δ is found to be initially higher than the other results, followed by a fall with increasing β and then a raise in δ again. This is not the case for the 3D CFD results which closely follow the experimental trend to within 2° of the LDA data with a continual increase of δ with increasing β . Further examination of the 2D CFD results at lower values of β showed this discrepancy to be caused by excessive entrainment of the secondary jet into the primary jet causing the primary jet to expand more rapidly. This expansion process resulted in a smaller recirculation zone and thus a greater primary jet deflection δ . As the value of β increased, however, less entrainment of the secondary jet occurred with a subsequent increase in adjacent recirculation zone diameter. Thus at this point, there is actually a fall in primary jet deflection δ as can be seen in Figure 1a. Finally once the secondary jet has attained sufficient momentum, a mechanism similar to that in the actual 3D system occurred where the secondary jet opposes the cross flow in the region above the jet resulting in movement of the attachment point of the primary jet up towards the jet exit with increased values of δ . Therefore although the 2D model has been previously successful in predicting oscillatory behaviour without secondary injection ($\beta = 0$), with secondary injection the model is less reliable. In contrast, the 3D CFD model reliably predicts the jet deflection characteristics under all the injection conditions of β tested.

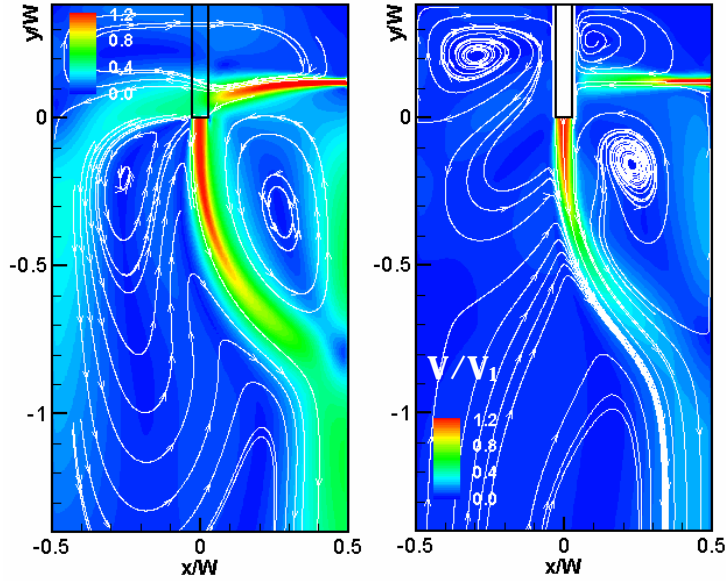
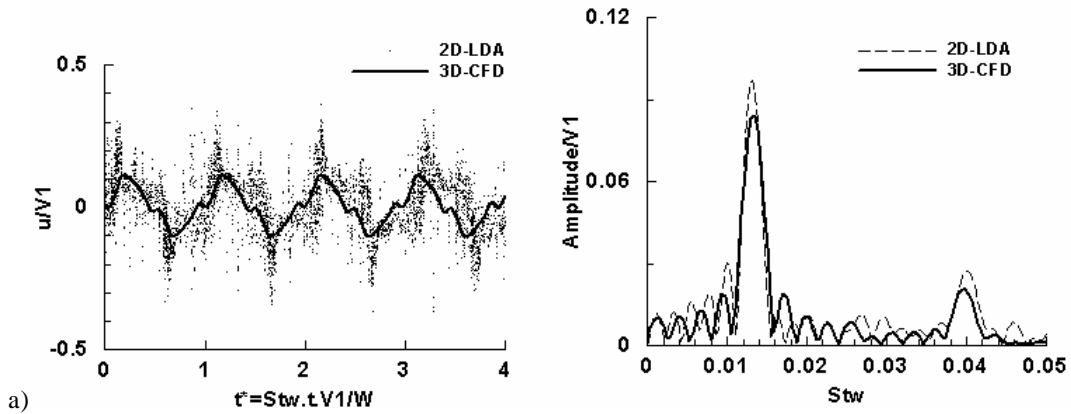


Fig. 10. CFD results ($Y_1/W = 0.12$, $\mathbf{b} = 48.2\%$) a) 2D model b) 3D model

4.3 Primary jet flow temporal characteristics with injection ($\mathbf{b} > 0$)

Figure 11 shows the effect of increasing secondary momentum β on the LDA and 3D CFD time series and spectral characteristics of the primary jet. The monitoring point was set to $x=0$, $y/W = -0.6$, $z = 0$. With no secondary injection, i.e. $\beta = 0$ (Figure 11a), the jet in both the CFD and LDA characteristics oscillates as expected with a dominant frequency corresponding to a Strouhal number of $St_w \approx 0.013$. With secondary injection of $\beta = 24\%$ (Figure 11b), the jet attains a mean position corresponding to a jet deflection of around $\delta = 17^\circ$. The corresponding cross flow data and zero frequency peak also indicate a mean positive cross flow velocity of around 10% of V_1 . This is representative of the mean deflection of the flow away from the centreline of the cavity. The primary jet, however, still has unsteady characteristics although there is no single dominant frequency as in the case of no secondary injection. There is also no significant correlation between the CFD and LDA cross flow data with the LDA data containing bursts of higher cross flow velocities at irregular intervals.



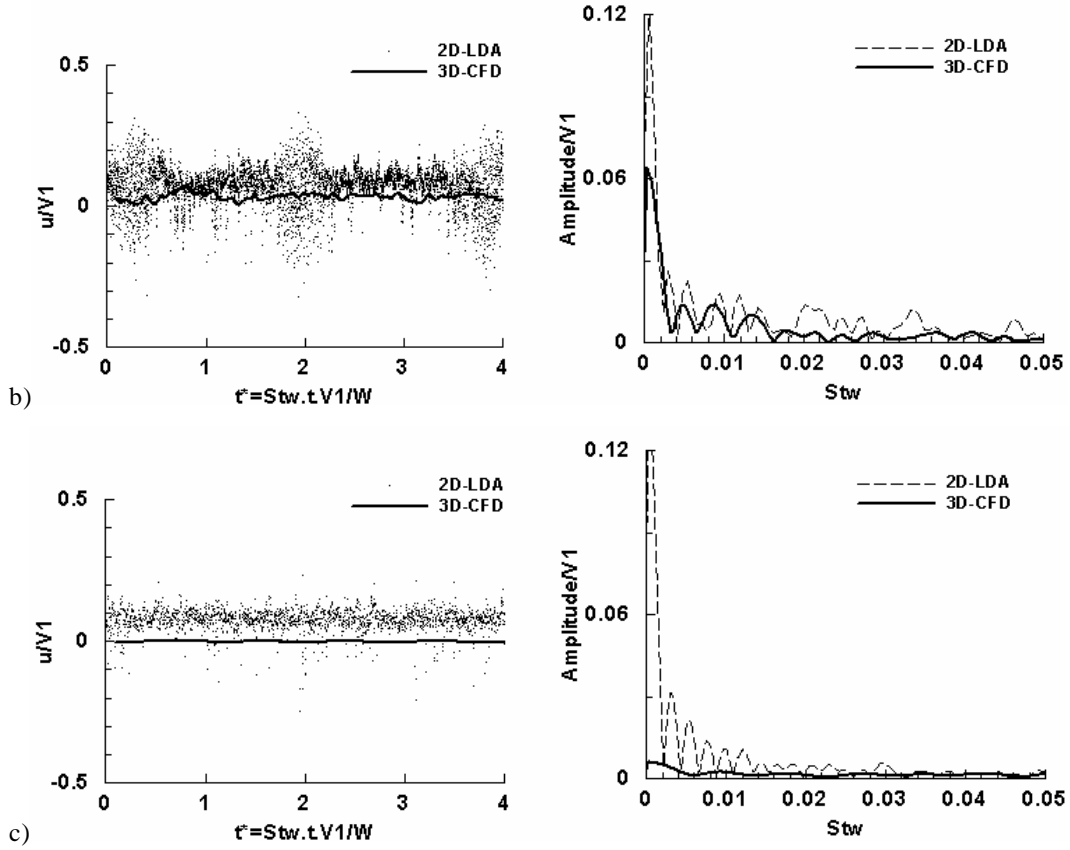


Fig. 11. LDA and 3D CFD spectral characteristics of the jet ($V_1 = 3.75\text{m/s}$, $Y_1/W = 0.12$) a) $\beta = 0$ b) $\beta = 24\%$ c) $\beta = 49\%$

With an increase in $\beta = 49\%$ (Figure 11c), the unsteadiness of the primary jet is reduced further with smaller cross flow amplitudes than at $\beta = 24\%$. Therefore although the mean characteristics of the system are providing the required jet deflections, the cross flow results indicate that the primary jet is still moving transversely across the cavity. If the amplitude of the cross flow is representative of jet movement, the LDA data also suggests the jet unsteadiness reduces with increasing secondary injection β . This general cross flow trend appears to be captured by the 3D CFD.

4.4 Control sensitivity

Results in Figure 1 for increases in β above 20%, in terms of δ the mean flow deflection sensitivity is reduced. Also, the mean jet flow deflection angle is shown to be insensitive to secondary jet momentum rates below $\beta \approx 4.5\%$. Mean jet flow reattachment points and secondary jet momentum rates can be represented by the semi-empirical equation in Eq. (7) obtained from regression of the measured data, where the constants $a = 0.335$ and $b = 1.116$ at $Y_1/W = 0.12$.

$$\frac{Y_R}{W} = \left[\text{Ln}(e^b \cdot b^a) \right]^{-1} \quad (7)$$

The prediction of the mean flow deflection angle is then possible by simply applying Eq. (7) to the predicted value of Y_R for a given β . This semi-empirical approach to the problem has allowed extrapolation of the measured data to any given value. Further analysis of Eq. (7) allows predictions of the flow control limits for the method. Thus control sensitivity of the flow to secondary injection can be determined by noting that Y_R approaches infinity (i.e. zero primary jet deflection) as β decreases towards a threshold value such that

$$b_{\text{threshold}} = e^{-\frac{b}{a}} \quad (8)$$

where the value of β must be greater than the threshold value for effective deflection of the mean jet flow. As β increases, Y_R decreases towards a mathematical limit of zero. Table 1 summarises these values at the three injection points above and below the nozzle.

i	Y/W	$b_{\text{threshold}} [\%]$	$b_{D(YR/W)<2\%} [\%]$	$(Y_R/W)_{\beta=1}$	$d_{\beta=1} [^\circ]$
1	0.12	3.6	25.5	0.9	29.2
2	-0.28	10.8	39.0	1.2	23.3
3	-0.68	8.7	35.6	1.0	25.9

Table 1 – Summary of vectoring performance for different positions of secondary injection

The results show, higher vectoring angles were achieved for the first position of injection for values of β_1 within 3.6%–25.5%, than those below the nozzle exit of 10.8% < β_2 < 39.0% and 8.7% < β_3 < 35.6%. Thus vectoring performance with low secondary jet momentum was clearly improved for injection above the nozzle exit. At higher values of β this configuration was still observed to have superior performance and extrapolated data showed higher angles of flow deflection for equal secondary and primary injection momentum rates, i.e., $\beta=1$. A mean primary jet flow deflection angle of $\delta_1=29.2^\circ$ is expected, which is greater than the extrapolated values of $\delta_2=23.3^\circ$ and $\delta_3=25.9^\circ$ for the other two vectoring configurations.

5. SUMMARY

A method of thrust vector control has been demonstrated based on manipulation of a low Strouhal number ($St < 0.02$), self-sustained oscillatory turbulent bound jet. The jet is bound by injection into a rectangular cavity. Thrust vector control has been achieved by secondary injection of mass flow from a lateral jet positioned on one of the cavity sidewalls. A combined LDA and CFD study was completed for a range of secondary injection conditions and positions.

The 2D CFD model generally gave acceptable predictions of thrust vectoring characteristics for low secondary momentum injections (<10% of primary jet momentum). But due to the 3D flow effects poor predictions of thrust vectoring performance were obtained for higher secondary momentums at any injection position. The 3D CFD model, however, predicted the thrust vectoring performance of the primary jet to within 2° of all tested conditions. Issues still remain through with the transient CFD characteristics with respect to cross flow unsteadiness.

Maximum thrust and good vectoring performance in terms of control sensitivity was achieved when injecting secondary momentum above the nozzle exit. This mechanism involved direct manipulation of the cross flow feedback loop linking the two recirculation zones bounding the primary jet. When injecting at this position, maximum performance was achieved when limiting the secondary momentum to less than 25% of the primary jet momentum with a 17° primary jet deflection. A further 6° of vectoring angle was possible for double the secondary momentum injection.

Future work aims to investigate replacing the mass flow injection system with a zero net mass flux injection method such as a synthetic jet system.

REFERENCES

- Alvi F.S., Strykowski P.J., Krothapalli A. and Forliti D.J., *Vectoring thrust in multiaxes using confined shear layers*. Journal of Fluids Engineering, Vol. 122, No. 1, pp. 3-13, 2000.
- Durst, F.; Melling, A. & Whitelaw, J.H. 1981 *Principles and Practice of Laser Doppler Anemometry*. Second Edition. London: Academic Press.
- Fletcher, C.A.J., *Computational Techniques for Fluid Dynamics: Fundamentals and General Techniques*. Vol. 1. 2001, New York: Springer-Verlag.

- Gebert, B.M., M.R. Davidson, and M.J. Rudman, *Computed oscillations of a confined submerged liquid jet*. Applied Mathematical Modelling, 1998. 22: p. 843-850.
- Kim, S.-E. and D. Choudhury "A Near-Wall Treatment Using Wall Functions Sensitized to Pressure Gradient." ASME Fluids Engineering Division 217 (Separated and Complex Flows). (1995)
- Launder, B. E. and D. B. Spalding. *Mathematical models of turbulence*. Academic press. (1972)
- Launder, B. E. and D. B. Spalding. *The numerical computation of turbulent flows*. Computer Methods in Applied Mechanics and Engineering 3: 269-289. (1974)
- Lawson N.J., Davidson M.R. Crossflow Characteristics of an Oscillating Jet in a Thin Slab Caster, *Journal of Fluids Engineering* 121, p589-595 (1999).
- Lawson, N.J. and M.R. Davidson. *An investigation of a low Strouhal number oscillatory jet submerged in a thin rectangular cavity*. in *10th International Symposium on Application of Laser Techniques on Fluid Mechanics*. 2000. Lisbon, Portugal.
- Lawson, N.J. and M.R. Davidson, *Self sustained oscillation of a submerged jet in a thin rectangular cavity*. Journal of Fluids and Structures, 2001. 15: p. 59-81.
- Miller, D.N., P.J. Yagle, and J.W. Hamstra. *Fluidic Throat Skewing for thrust vectoring in fixed geometry nozzles*. in *37th AIAA Aerospace Sciences Meeting and Exhibit*. 1999. Reno, NV.
- Pack, L.G. and A. Seifert, *Periodic excitation for jet vectoring and enhanced spreading*. Journal of Aircraft, 2001. 38(3): p. 486-495.
- Raman, G. and E.J. Rice, *Development of phased twin flip-flop jets*. Journal of Vibration and Acoustics, 1994. 116: p. 263-267.
- Raman, G., *Using control unsteady fluid mass addition to enhance jet mixing*. AIAA Journal, 1997. 35(4): p. 647-656.
- Rockwell, D., *Oscillations of impinging shear layers*. AIAA Journal, 1983. 21(5): p. 645-664.
- Rockwell, D. and E. Naudascher, *Review - Self sustained oscillations of flow past cavities*. Journal of Fluids Engineering, 1978. 100: p. 152-165.
- Rockwell, D. and E. Naudascher, *Self sustained oscillations of impinging free shear layers*. Ann. Rev. Fluid Mech., 1979. 11: p. 67-94.
- Schmid G.F., Strykowski P.J., Madruga M., Das D. and Krothapalli A., *Jet attachment behavior using counterflow thrust vectoring*. Proceedings of 13th ONR Propulsion Conference, Minneapolis, MN, Aug., 10-12, pp. 63-68, 2000
- Shakouchi, T., Y. Suematsu, and T. Ito, *A Study on Oscillatory Jet in a Cavity*. Bulletin of the JSME, 1982. 29(206).
- Shakouchi, T., S. Kuzuhara, and J. Yamaguchi, *Oscillatory phenomena of an attached jet*. Bulletin of the JSME, 1986. 29(250): p. 1117-1123.
- Shih, T.-H., W. W. Liou, et al. *A New k-ε Eddy-Viscosity Model for High Reynolds Number Turbulent Flows - Model Development and Validation*. Computers Fluids 24(3): 227-238. (1995).
- Smith, B.L. and A. Glezer. *Vectoring and small scale motions effect in free shear flows using synthetic jet actuators*. in *35th AIAA Aerospace Sciences Meeting*. 1997. Reno, NV.